

# Insight into the Binding of Antifreeze Proteins to Ice Surfaces via $^{13}\text{C}$ Spin Lattice Relaxation Solid-State NMR

Youngang Mao and Yong Ba

Department of Chemistry and Biochemistry, California State University, Los Angeles, Los Angeles, California 90032

**ABSTRACT** The primary sequences of type I antifreeze proteins (AFPs) are Ala rich and contain three 11-residue repeat units beginning with threonine residues. Their secondary structures consist of  $\alpha$ -helices. Previous activity study of side-chain mutated AFPs suggests that the ice-binding side of type I AFPs comprises the Thr side chains and the conserved  $i + 4$  and  $i + 8$  Ala residues, where  $i$  indicates the positions of the Thrs. To find structural evidence for the AFP's ice-binding side, a variable-temperature dependent  $^{13}\text{C}$  spin lattice relaxation solid-state NMR experiment was carried out for two Ala side chain  $^{13}\text{C}$  labeled HPLC6 isoforms of the type I AFPs each frozen in  $\text{H}_2\text{O}$  and  $\text{D}_2\text{O}$ , respectively. The first one was labeled on the equivalent 17th and 21st Ala side chains ( $i + 4, 8$ ), and the second one on the equivalent 8th, 19th, and 30th Ala side chains ( $i + 6$ ). The two kinds of labels are on the opposite sides of the  $\alpha$ -helical AFP. A model of Ala methyl group rotation/three-site rotational jump combined with water molecular reorientation was tested to probe the interactions of the methyl groups with the proximate water molecules. Analysis of the  $T_1$  data shows that there could be 10 water molecules closely capping an  $i + 4$  or an  $i + 8$  methyl group within the range of van der Waals interaction, whereas the surrounding water molecules to the  $i + 6$  methyl groups could be looser. This study suggests that the side of the  $\alpha$ -helical AFP comprising the  $i + 4$  and  $i + 8$  Ala methyl groups could interact with the ice surface in the ice/water interface.

## INTRODUCTION

Antifreeze proteins (AFPs) (1–4) exist in the serums of certain species of fish (5), insects (6), and plants (7,8) living in subzero environments. It is known that AFPs depress the freezing points of their aqueous solutions noncolligatively through ice-growth inhibition (9,10). Among all types of AFPs, HPLC6 isoform of type I antifreeze proteins (11) isolated from the blood serum of winter flounder is the most intensively studied one. It has an alanine-rich (>60%) primary sequence containing three 11-residue repeat units starting with threonine residues. Its secondary structure is of an  $\alpha$ -helix (12–14).

Earlier proposed mechanisms to explain the ice growth inhibition include adsorption inhibition (15) and Kelvin effect (16). The well-known ice etching experiment (17, 18) identified that HPLC6 peptides bind to the 12 equivalent bipyramidal planes  $\{2\ 0\ 2\ 1\}$  of the hexagonal ice (ice Ih). The distance between the periodicity in ice oxygen repeat length was found to nearly match with the repeat unit of the 11 amino acids. It was proposed that the side chains from the Thr-2/Asp-5, Leu-12/Thr-13/Asn-16, Leu-23/Thr-24/Asn-27, and Thr-35 groups form the ice-binding motifs through hydrogen bonding interactions (12). To examine the importance of hydrogen bonding, systematic side-chain mutations on Thr residues were carried out (19–21). The results, however, suggest that van der Waals interaction is the primary determinant for the AFP's binding to the ice surfaces whereas hydrogen bonding only plays a minimal role.

Another activity study, where Leu and Asn residues were substituted, suggests that the primary role for Leu is to prevent peptide aggregation, and the role for Asn is to enhance aqueous solubility rather than being involved in stereospecific hydrogen bonding (22). A comparison of the primary sequences of five type I isoforms from right-eye flounders showed that Leu and Asx of the putative ice-binding motifs are not well conserved (23). The importance of Ala residues was, therefore, investigated by substituting Leu for Ala at positions around the helix to identify the ice-binding sites by steric interference. It was observed that replacement of Alas by Leus at position 19 or 20 resulted in insignificant loss in antifreeze activity. However, replacement at position 17 or 21 only retained minor antifreeze activity. Thus, it was proposed that the ice-binding side for a type I AFP comprises the Thr side chains and the conserved  $i + 4$  and  $i + 8$  Ala residues, where  $i$  indicates the position of a Thr commencing the repeat unit of the 11 amino acids. It appears that the AFP's binding to the ice surfaces primarily attribute to the van der Waals interaction. This interaction is much weaker than the previously proposed hydrogen bonding interaction. It was later on found that the binding of a type I AFP to the ice surfaces is reversible (24) being in favor of the weaker van der Waals interaction.

To find structural evidence for the AFP's ice-binding side, variable temperature-dependent  $^{13}\text{C}$  spin lattice relaxation solid-state NMR experiment was carried out for two Ala side-chain  $^{13}\text{C}$ -labeled HPLC6 isoforms of the type I AFPs each frozen in  $\text{H}_2\text{O}$  and  $\text{D}_2\text{O}$ , respectively. The first one was labeled on the equivalent 17th and 21st Ala side chains ( $i + 4, 8$ ), and the second one on the equivalent 8th, 19th, and 30th Ala side chains ( $i + 6$ ). The  $^{13}\text{C}$ -labeled positions in the

Submitted July 25, 2005, and accepted for publication April 10, 2006.

Address reprint requests to Yong Ba, Tel.: 323-343-2360; Fax: 323-343-6490; E-mail: yba@calstatela.edu.

© 2006 by the Biophysical Society

0006-3495/06/08/1059/10 \$2.00

doi: 10.1529/biophysj.105.071316

first peptide comprise alanine residues in the proposed ice-binding side, but the second one is with the alanine residues on the opposite side. A model of Ala methyl group rotation/three-site rotational jump combined with water molecular reorientation was tested to probe the interactions of the methyl groups with the proximate water molecules. This model provides a means to probe the dynamics of the methyl group's rotations, and their water surroundings including the proximity, the number of water molecules and their dynamics.

## EXPERIMENTAL SECTION

### Sample preparation

The primary sequence of the HPLC6 isoform consists of Asp-Thr-Ala-Ser-Asp-Ala-Ala-Ala-Ala-Ala-Leu-Thr-Ala-Ala-Asn-Ala-Lys-Ala-Ala-Ala-Glu-Leu-Thr-Ala-Ala-Asn-Ala-Ala-Ala-Ala-Ala-Ala-Ala-Thr-Ala-Arg. It has three 11-residue repeat units commencing with the threonine residues. Its secondary structure consists of an  $\alpha$ -helix. Two Ala methyl group  $^{13}\text{C}$ -labeled samples were used for this study. One sample was labeled at the positions 17 and 21 (sample AFP  $i + 4, 8$ ) and the other at the positions 8, 19, and 30 (sample AFP  $i + 6$ ). As reviewed in the introduction, the  $^{13}\text{C}$ -labeled methyl groups in the AFP  $i + 4, 8$  sample are the suggested residues to interact with the ice surface. Crystal structure shows that all of the  $i + 4$  and  $i + 8$  alanine residues are in one flat surface and a pair of the  $i + 4$  and  $i + 8$  alanine residues has a local C2 symmetry with the axis perpendicular to the surface between the two residues. Thus, their local structures are equivalent in terms of mirror symmetry, which gives equal isotropic NMR parameters. The two labeled positions are indicated with the C13 signs in the  $\alpha$ -helical structure given in Fig. 1. The  $^{13}\text{C}$ -labeled positions in the AFP  $i + 6$  sample are on the opposite side. Owing to the periodical structure, the 8, 19, and 30 residues are equivalent in terms of their local structures as shown in Fig. 1. The advantage to use the multi-labeled peptides is from their stronger  $^{13}\text{C}$  NMR signals, whereas the differ-

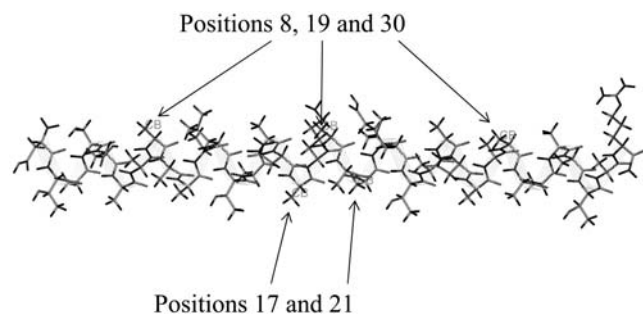


FIGURE 1  $\alpha$ -Helical structure of the type I AFP, where the Ala  $^{13}\text{C}$ -labeled methyl groups are indicated.

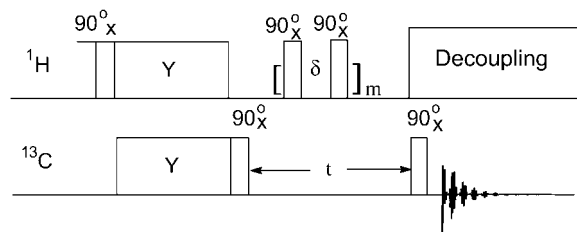
ences in NMR parameters for the locally equivalent  $^{13}\text{C}$  spins are insignificant.

The  $^{13}\text{C}$ -labeled peptides were provided by Auspep (Parkville Australia). The C-termini of them were capped with carboxyl amides. Their mass spectra show that the purity for the AFP  $i + 4, 8$  peptide is  $\geq 93\%$  and that for the AFP  $i + 6$  peptide is  $\geq 95\%$ . Two AFP samples, one frozen in  $\text{H}_2\text{O}$  and the other in  $\text{D}_2\text{O}$ , were prepared for each of the peptides; 5 mg of a dried AFP was added into a 7 mm solid state NMR rotor, and 0.2 ml water was added to dissolve the peptides. Freeze-dried peptides from  $\text{D}_2\text{O}$  solutions were used to prepare the  $\text{D}_2\text{O}$  samples to eliminate the amount of protons exchanged from the peptides to the solutions. After a solution was made, the NMR rotor was tightly sealed with a Teflon O-ring cap. The sample was then frozen using liquid nitrogen. Afterward, the sample was placed in a freezer at  $-20^\circ\text{C}$  to allow the water molecules and the peptides to relax overnight at a temperature much higher than the glass transition temperature of ice Ih (which is about  $-125^\circ\text{C}$ ). An experiment on the formation of a gas hydrate shows that water molecules are able to perform local reorientation and diffusion to adjust their local structure to be energetically stable (25). The relaxation process would result in the water surroundings for a peptide in favor of the lowest energy. Thermal hysteresis study of AFPs uses a method to quickly freeze an AFP to  $-40^\circ\text{C}$ , and then heat the sample to a temperature below  $0^\circ\text{C}$  (26). No protein denature in the secondary structure caused by the freezing process was reported in literature. Since freeze quenching is usually used to preserve a molecular structure in solution, we believe the  $\alpha$ -helical structure of the type I AFP was not likely to be altered by the freezing process using liquid nitrogen.

### $T_1$ NMR experiment

The NMR data were collected with a Bruker (Karlsruhe, Germany) Avance DRX 400 NMR Spectrometer using a 7 mm double resonance MAS (magic angle spinning) probe. The  $T_1$  experiments were carried out at  $-10, -20, -30, -40,$  and  $-50^\circ\text{C}$ . CP (cross-polarization) contact time of 700  $\mu\text{s}$ ,  $90^\circ$  pulse length of 7  $\mu\text{s}$ , and MAS rate of 2 kHz were used. From 512 to 1024 scans were used to collect the NMR signals. Proton high power decoupling (HPDec) was employed during the acquisition period. Adamantane and glycine solid powders were used to adjust the CP Hartman-Hahn condition and also as the secondary external references for the  $^{13}\text{C}$  chemical shifts.

The CP MAS HPDec  $^{13}\text{C}$   $T_1$  NMR pulse sequence is shown in Fig. 2 (27) where the radio frequency phase and the receiver phase cycling ( $x, y, -x, -y$ ) were used. To eliminate the transient nuclear Overhauser effect, proton transitions were saturated during the  $T_1$  recovering period by using a train of weak  $90^\circ$  pulses with equal intervals of  $\delta = 3$  ms (27,28). A single-exponential decay curve for the recovery of the  $^{13}\text{C}$  signal can be described as

FIGURE 2 CP MAS HPDec  $^{13}\text{C}$   $T_1$  solid-state NMR experiment.

$$S_z(t) = [S_z(0) - S_z(\infty)]\text{Exp}\left(-\frac{t}{T_{1\text{C}}}\right) + S_z(\infty), \quad (1)$$

where  $S_z(0)$  denotes the magnetization at time zero,  $S_z(\infty)$  that after having approached equilibrium, and  $T_{1\text{C}}$  the  $^{13}\text{C}$  spin lattice relaxation time.

### $T_1$ THEORETICAL MODEL

$T_1$  theory due to molecular-orientation in solids can be found in literature (28–30). A  $T_1$  model specifically for a methyl group rotation can also be found in Naito and McDowell (31). However, in this reference, the molecular axes are fixed and the direction of the magnetic field is varied for the calculation, which makes it inconvenient to do integration for molecular orientations over a solid powder. In this section, we will derive an alternative formula to facilitate the integration for a solid powder. Another critical problem that we will address is the effect of the variation of an internuclear distance with time on the spin lattice relaxation rate. As will be seen, besides the angular change for the  $^1\text{H}$ - $^{13}\text{C}$  internuclear vector due to the reorientation of surrounding water molecules to a methyl  $^{13}\text{C}$ , it also involves time-dependent internuclear distance change. Bloembergen and Abragam (32,33) addressed the spectral density function for a translational motion over a solid crystal. Here, we will discuss how to incorporate both the rotational motion and the translational motion into a single spectral density function.

### Relaxation rate

We will refer to reference (34) to give a general expression for a relaxation rate. The Hamiltonian of dipolar interaction for a heteronuclear two-spin (AX) system can be written as

$$H_{\text{dd}} = \sum_{m=-2}^2 Y_{2,m} A_m \hbar^2 \gamma_A \gamma_X \Gamma_{\text{AX}}^{-3} \frac{\mu_0}{4\pi} \quad (2)$$

where  $\gamma_A$  and  $\gamma_B$  denote the magnetogyric ratios of nuclei A and X, respectively,  $\mu_0$  the permeability of a vacuum, and  $r_{\text{AX}}$  the displacement between the A and X nuclei.  $Y_{2,m}$  terms represent the second-order spherical harmonics determining the orientational dependence, and  $A_m$  terms the spin dependence of the dipolar interaction. Following the time-

dependent perturbation theory, the transition rate can be found to be

$$R_{\text{rs}} = (2\pi C_0)^2 N_X \sum_m \overline{\langle \psi_r | A_m | \psi_s \rangle^2} \times \int_{-\infty}^{\infty} r_{\text{AX}}^{-3}(t'' + \tau) Y_{2,m}(t'' + \tau) r_{\text{AX}}^{-3}(t'') Y_{2,m}(t'') \times \exp(-i\omega_{\text{rs}}\tau) d\tau, \quad (3)$$

where  $\omega_{\text{rs}}$  denotes the angular frequency of the corresponding transition, the horizontal bar indicates the ensemble average,  $C_0 = \frac{\mu_0}{4\pi} \gamma_A \gamma_X \frac{\hbar}{2\pi}$ , and  $N_X$  accounts for the number of X spins. Since an autocorrelation function can be defined as

$$G_m(\tau) = \overline{N_X r_{\text{AX}}^{-3}(t'' + \tau) Y_{2,m}(t'' + \tau) r_{\text{AX}}^{-3}(t'') Y_{2,m}(t'')}, \quad (4)$$

the relaxation rate can be written as

$$R_{\text{rs}} = (2\pi C_0)^2 \sum_m \overline{\langle \psi_r | A_m | \psi_s \rangle^2} J_m(\omega) \quad (5)$$

where

$$J_m(\omega) = \int_{-\infty}^{\infty} G_m(\tau) \exp(-i\omega_{\text{rs}}\tau) d\tau \quad (6)$$

is defined as the spectral density function which is strongly dependent on the mode of a molecular motion.

### Rotational motion

For a fixed internuclear distance,  $r_{\text{AX}}(t) = r_{\text{AX},0}$ , thus  $r_{\text{AX}}^{-3}(t'' + \tau) r_{\text{AX}}^{-3}(t'') = r_{\text{AX},0}^{-6}$ .  $G_m(\tau)$  in Eq. 4 becomes the rotational autocorrelation function

$$G_{\text{R}}(\tau) = N_X r_{\text{AX},0}^{-6} |C_{2,m}|^2 G_{\text{r}}(\tau) = N_X r_{\text{AX},0}^{-6} |C_{2,m}|^2 \exp(-|\tau|/\tau_{\text{c}}). \quad (7)$$

Thus, the spectral density function for a molecular reorientation can be written as

$$J_{\text{m,R}} = \frac{N_X r_{\text{AX},0}^{-6} C_{2,m}^2 \tau_{\text{c}}}{1 + \omega^2 \tau_{\text{c}}^2}. \quad (8)$$

Following the general procedure (34), the  $^{13}\text{C}$  spin lattice relaxation rate can be found to be

$$T_{1\text{C}}^{-1} = \frac{N_X (2\pi D_0)^2 \tau_{\text{c}}}{10} \left[ \frac{C_{2,0}^2}{1 + (\omega_X - \omega_A)^2 \tau_{\text{c}}^2} + \frac{3C_{2,\pm 1}^2}{1 + \omega_A^2 \tau_{\text{c}}^2} + \frac{6C_{2,\pm 2}^2}{1 + (\omega_X + \omega_A)^2 \tau_{\text{c}}^2} \right], \quad (9)$$

where  $D_0 = \frac{\mu_0}{4\pi} r_{\text{AX},0}^{-3} \gamma_A \gamma_X \frac{\hbar}{2\pi}$ . For a solid powder, the spatial average  $\langle T_{1\text{C}}^{-1} \rangle$  can be obtained by integration over the angle  $\beta$  defined as between an axis describing the molecular orientation and the direction of the external magnetic field. Thus,

$$\begin{aligned} \langle T_{1C}^{-1} \rangle &= \frac{N_X (2\pi D_0)^2 \tau_c}{10} \int_0^\pi \left[ \frac{C_{2,0}^2(\beta)}{1 + (\omega_X - \omega_A)^2 \tau_c^2} \right. \\ &\quad \left. + \frac{3C_{2,\pm 1}^2(\beta)}{1 + \omega_A^2 \tau_c^2} + \frac{6C_{2,\pm 2}^2(\beta)}{1 + (\omega_X + \omega_A)^2 \tau_c^2} \right] \\ &\quad \times \frac{1}{2} \sin \beta d\beta. \end{aligned} \quad (10)$$

To do the integration, the second order spherical harmonics

$$\begin{cases} Y_{2,0} = \sqrt{\frac{5}{4}}(1 - 3\cos^2\theta) \\ Y_{2,\pm 1} = \sqrt{\frac{15}{2}}\cos\theta\sin\theta\exp(\pm i\varphi) \\ Y_{2,\pm 2} = -\sqrt{\frac{15}{8}}\sin^2\theta\exp(\pm 2i\varphi) \end{cases} \quad (11)$$

and the transition probabilities

$$\langle \psi_r | A_m | \psi_s \rangle^2 = \begin{cases} 1/20 & \text{for } W_0 \\ 3/40 & \text{for } W_1 \\ 3/10 & \text{for } W_2 \end{cases} \quad (12)$$

have been used.  $\theta$  in Eq. 11 defines the angle between the internuclear vector and the direction of the static magnetic field  $\mathbf{B}_0$ , and  $\phi$  the longitude in the spherical coordination. Because  $|\exp(\pm ni\varphi)|^2 = 1$  ( $n = 1, 2$ ),  $|C_{2,m}|^2$  terms can be found to be

$$\begin{cases} C_{2,0}^2 = \frac{5}{4}[1 - 6\langle \cos^2\theta \rangle + 9\langle \cos^4\theta \rangle] \\ C_{2,\pm 1}^2 = \frac{15}{2}[\langle \cos^2\theta \rangle - \langle \cos^4\theta \rangle] \\ C_{2,\pm 2}^2 = \frac{15}{8}(1 - 2\langle \cos^2\theta \rangle + \langle \cos^4\theta \rangle). \end{cases} \quad (13)$$

### Translational motion

For translational motion,  $G_m(\tau)$  becomes the product of the translational autocorrelation function  $G_T(\tau) = \overline{N_X r_{AX}^{-3}(t'' + \tau) r_{AX}^{-3}(t'')}$  and the factor  $|Y_{2,m}(0)|^2 = 1$ , therefore

$$R_{rs} = (2\pi C_0)^2 \sum_m \overline{\langle \psi_r | A_m | \psi_s \rangle^2} J_{m,T}(\omega), \quad (14)$$

where

$$J_{m,T}(\omega) = \int_{-\infty}^{\infty} G_T(\tau) \exp(-i\omega_s \tau) d\tau \quad (15)$$

is the spectral density of the translational motion. Bloembergen and Abragam (32,33) assume that the translational correlation function for a two spin interaction is proportional to  $\exp(-|\tau|/\tau_c)$ , thus,

$$J_{m,T}(\omega) = \frac{16\pi n}{15} \int_{r_{AX,\min}}^{\infty} \frac{dr_{AX}}{r_{AX}^4} \frac{\tau_c}{1 + \omega^2 \tau_c^2}, \quad (16)$$

where,  $\tau_c = \frac{r_{AX}^2}{6D}$  defines the correlation time of the translational motion,  $n$  is the spin number per unit volume in the translational range of spin  $X$ ,  $D$  is the diffusion coefficient, and  $r_{AX,\min}$  is the nearest distance that the  $X$  spin can

approach to the  $A$  spin. Thus, the relaxation rate can be found to be

$$\begin{aligned} \frac{1}{T_{1C}} &= W_0 + 2W_1 + W_2 \\ &= \frac{1}{20} (2\pi C_0)^2 [J_{0,T}(\omega_X - \omega_A) + 3J_{\pm 1,T}(\omega_A) \\ &\quad + 6J_{\pm 2,T}(\omega_X + \omega_A)]. \end{aligned} \quad (17)$$

### Coexistence of rotational and translational motions

In this case,  $G_m(\tau)$  in Eq. 4 depends on both molecular orientation and translational motions. Because  $\overline{Y_{2,m}(t'' + \tau) Y_{2,m}(t'')}$  only depends on the angular coordinates  $\theta$  and  $\phi$ , and  $\overline{N_X r_{AX}^{-3}(t'' + \tau) r_{AX}^{-3}(t'')}$  only on  $r$ , they can be averaged independently over their corresponding variables resulting in

$$\begin{aligned} G_m(\tau) &= \overline{N_X r_{AX}^{-3}(t'' + \tau) Y_{2,m}(t'' + \tau) r_{AX}^{-3}(t'') Y_{2,m}(t'')} \\ &= \overline{Y_{2,m}(t'' + \tau) Y_{2,m}(t'')} \overline{N_X r_{AX}^{-3}(t'' + \tau) r_{AX}^{-3}(t'')} \\ &= |C_{2,m}|^2 \overline{G_r(\tau) N_X r_{AX}^{-3}(t + \tau) r_{AX}^{-3}(t)} \\ &= |C_{2,m}|^2 G_{m,R,T}(\tau), \end{aligned} \quad (18)$$

where  $G_r(\tau)$  is defined as the rotational autocorrelation function, and  $G_{m,R,T}(\tau)$  the joint rotational-translational correlation function. If the translational and rotational motions come from a unique source, we have just one correlation time  $\tau_c = \tau_R = \tau_T$ . We assume this being the situation. Bloembergen and Abragam (33) assume that the translational correlation function  $\overline{N_X r_{AX}^{-3}(t'' + \tau) r_{AX}^{-3}(t'')}$  takes a single exponential function, i.e.,  $\overline{r_{AX}^{-3}(t'' + \tau) r_{AX}^{-3}(t'')} = \overline{r_{AX}^{-3}(t) r_{AX}^{-3}(t)} \exp(-|\tau|/\tau_c)$ . Thus,  $G_{m,R,T}(\tau)$  can be written as

$$\begin{aligned} G_{m,R,T}(\tau) &= \overline{G_r(\tau) N_X r_{AX}^{-3}(t + \tau) r_{AX}^{-3}(t)} \\ &= \overline{N_X} \exp(-|\tau|/\tau_c) \overline{r_{AX}^{-3}(t) r_{AX}^{-3}(t)} \exp(-|\tau|/\tau_c) \\ &= \overline{N_X r_{AX}^{-3}(t) r_{AX}^{-3}(t)} \exp(-\tau/(\tau_c/2)) \end{aligned} \quad (19)$$

and the transition rate can be written as

$$\begin{aligned} R_{rs} &= (2\pi C_0)^2 \sum_m \overline{\langle \psi_r | A_m | \psi_s \rangle^2} \int_{-\infty}^{\infty} |C_{2,m}|^2 G_{m,R,T}(\tau) \\ &\quad \times \exp(-i\omega_s \tau) d\tau \\ &= (2\pi C_0)^2 \sum_m \overline{\langle \psi_r | A_m | \psi_s \rangle^2} |C_{2,m}|^2 J_{m,R,T}(\omega), \end{aligned} \quad (20)$$

where

$$J_{m,R,T}(\omega) = \frac{16\pi n}{15} \int_{r_{AX,\min}}^{\infty} \frac{1}{r_{AX}^4} \frac{\tau_c/2}{1 + \omega^2 \tau_c^2/4} dr_{AX}. \quad (21)$$

The final relaxation rate can be written as

$$\begin{aligned} \frac{1}{T_{1C}} &= W_0 + 2W_1 + W_2 \\ &= \frac{1}{20}(2\pi C_0)^2 [C_{2,0}^2 J_{0,R,T}(\omega_X - \omega_A) + 3C_{2,\pm 1}^2 J_{\pm 1,R,T}(\omega_A) \\ &\quad + 6C_{2,\pm 2}^2 J_{\pm 2,R,T}(\omega_X + \omega_A)]. \end{aligned} \quad (22)$$

For a solid powder, its spatial average takes the following form

$$\begin{aligned} \langle T_{1C}^{-1} \rangle &= \frac{1}{20}(2\pi C_0)^2 \int_0^\pi [C_{2,0}^2 J_{0,R,T}(\omega_X - \omega_A) \\ &\quad + 3C_{2,\pm 1}^2 J_{\pm 1,R,T}(\omega_A) + 6C_{2,\pm 2}^2 J_{\pm 2,R,T}(\omega_X + \omega_A)] \\ &\quad \times \frac{1}{2} \sin\beta d\beta. \end{aligned} \quad (23)$$

We are going to address three specific cases relevant to the spin lattice relaxation mechanisms for the Ala methyl  $^{13}\text{C}$  spins in the frozen AFP samples.

### Methyl group rotation and three-site rotational jump

Two mechanisms are significant to influence the Ala methyl  $^{13}\text{C}$   $T_1$  relaxation rate for the AFPs frozen in ice lattice. One is the methyl group rotation around the C-C chemical bond or three-site rotational jump around the C-C chemical bond if the energy barriers exist. The other is the reorientation of proximate water molecules to the methyl group. Other mechanism, such as arising from the peptide's tumbling like what is in a solution, is meaningless for a frozen sample. Effect due to other side-chain rotations in the same peptide is also insignificant due to the longer internuclear distance because the relaxation rate is inversely proportional to the sixth power of the internuclear distance.

Fig. 3 A schematically describes the model for a methyl group rotation, where the methyl carbon is positioned at the origin of the coordination,  $r_{\text{CH}}$  denotes the methyl C-H internuclear distance,  $\theta$  the angle between the magnetic field  $\mathbf{B}_0$  and the C-H vector,  $\beta$  the angle between the magnetic field and the C-C axis  $A$ ,  $\chi (= 72.3^\circ)$  the angle between the rotational axis  $A$  and the C-H vector, and  $\phi (= \omega t)$  the angle that the H has rotated with the angular frequency  $\omega$  at a time  $t$ . We can find

$$\cos\theta = \cos\chi\cos\beta + \sin\chi\sin\beta\cos\phi. \quad (24)$$

Thus,  $\langle \cos^2\theta \rangle$  and  $\langle \cos^4\theta \rangle$  terms have the following expressions:

$$\langle \cos^2\theta \rangle = \cos^2\chi\cos^2\beta + \frac{1}{2}\sin^2\chi\sin^2\beta \quad (25)$$

$$\begin{aligned} \langle \cos^4\theta \rangle &= \cos^4\chi\cos^4\beta + 3\cos^2\chi\cos^2\beta\sin^2\chi\sin^2\beta \\ &\quad + \frac{3}{8}\sin^4\chi\sin^4\beta. \end{aligned} \quad (26)$$

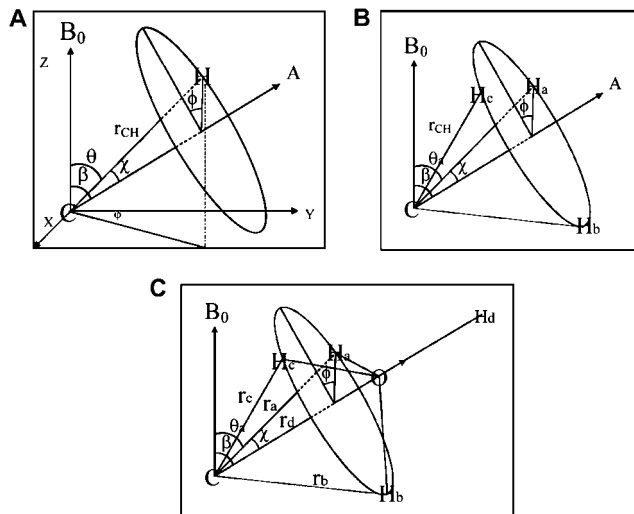


FIGURE 3 (A) Model of methyl group rotation. (B) Model of methyl group three-site rotational jump. (C) Model of water molecular reorientation.

To derive these equations, we have used  $\langle \cos^3\phi \rangle = 0$ , and  $\langle \cos^4\phi \rangle = 3/8$ .  $C_{2,m}^2$  terms in Eq. 13 are functions of  $\beta$ , thus the  $^{13}\text{C}$   $T_1$  values are orientation-dependent. The experimentally measured  $T_1$  value for a solid powder is the spatial average over  $\beta$  (from 0 to  $\pi$ ). Since  $\int_0^\pi |C_{2,m}^2|^2 \frac{1}{2} \sin\beta d\beta = 1$ . We found

$$\begin{aligned} \langle T_{1C}^{-1} \rangle &= \frac{N_X(2\pi D_0)^2 \tau_C}{10} \left[ \frac{1}{1 + (\omega_X - \omega_A)^2 \tau_C^2} + \frac{3}{1 + \omega_A^2 \tau_C^2} \right. \\ &\quad \left. + \frac{6}{1 + (\omega_X + \omega_A)^2 \tau_C^2} \right]. \end{aligned} \quad (27)$$

The model of three-site rotational jump is schematically shown in Fig. 3 B. We assume a hydrogen atom can jump with a single step among the three sites,  $a-c$ , through the C-C bond rotation. The equations for  $T_{1C}$  and  $\langle T_{1C} \rangle$  for this model were found to be the same as those for the model of methyl group rotation. Owing to this, we are not able to distinguish these two motional modes from the  $T_1$  data.

### Water molecular reorientation

Fig. 3 C shows the model of water molecular reorientation. It has been known that a water hydrogen atom in ice Ih can jump among the positions  $a-d$  through the reorientational motion along the other O-H bond (35, and Y. Ba, J. A. Ripmeester, and C. I. Ratcliffe, unpublished). The four positions form a tetrahedral geometry. We assume that water molecules surround the alanine methyl groups in the frozen peptide sample. The reorientational motion of the adjacent water molecules is able to cause the fluctuation of the local magnetic field for the methyl  $^{13}\text{C}$  spin. This introduces another mechanism for the  $^{13}\text{C}$  spin lattice relaxation. The effect of the water's reorientation is equivalent to a rotational motion plus a translational motion.

We use  $r_a$ ,  $r_b$ ,  $r_c$ , and  $r_d$  to denote the internuclear distances of these tetrahedral positions to the methyl carbon and  $\theta_a$ ,  $\theta_b$ ,  $\theta_c$ , and  $\theta_d$ , the angles between the C-H internuclear vectors and the external magnetic field. To simplify the calculation, we will use  $109.5^\circ$  for the H-O-H bond angle instead of the experimental value  $104.52^\circ$ . These internuclear distances were found to be

$$r_a = r_b = r_c = \sqrt{r_{\text{O-H}}^2 \sin^2(180^\circ - 109^\circ 28') + [r_{\text{C-O}} - r_{\text{O-H}} \cos(180^\circ - 109^\circ 28')]^2} \quad (28)$$

$$r_d = r_{\text{C-O}} + r_{\text{C-H}}, \quad (29)$$

where  $r_{\text{C-O}}$  denotes the internuclear distance between the methyl carbon nucleus and the water oxygen nucleus, and  $r_{\text{O-H}}$  is the water O-H bond length. The relations among these angles can be found to be

$$\cos\theta_a = \cos(\chi)\cos\beta + \sin(\chi)\sin\beta\cos(f_0) \quad (30)$$

$$\cos\theta_b = \cos(\chi)\cos\beta + \sin(\chi)\sin\beta\cos(f_0 + 120^\circ) \quad (31)$$

$$\cos\theta_c = \cos(\chi)\cos\beta + \sin(\chi)\sin\beta\cos(f_0 + 240^\circ) \quad (32)$$

$$\cos\theta_d = \cos\beta, \quad (33)$$

where

$$\cos\chi = \frac{[r_{\text{C-O}} - r_{\text{O-H}} \cos(180^\circ - 109^\circ 28')]}{\sqrt{(r_{\text{O-H}}^2 \sin^2(180^\circ - 109^\circ 28') + [r_{\text{C-O}} - r_{\text{O-H}} \cos(180^\circ - 109^\circ 28')]^2}} \quad (34)$$

$$\sin\chi = \frac{r_{\text{O-H}} \sin(180^\circ - 109^\circ 28')}{\sqrt{(r_{\text{O-H}}^2 \sin^2(180^\circ - 109^\circ 28') + [r_{\text{C-O}} - r_{\text{O-H}} \cos(180^\circ - 109^\circ 28')]^2}} \quad (35)$$

$$r_{\text{HH}} = 2r_{\text{O-H}} \sin(180^\circ - 109^\circ 28') \cos(60^\circ). \quad (36)$$

As shown in Fig. 3 C, the water reorientation causes both angular changes among  $\theta_a$ ,  $\theta_b$ ,  $\theta_c$ , and  $\theta_d$ , and radial changes from the smallest value  $r_{\text{CH,min}} = r_a = r_b = r_c$  to the largest value  $r_{\text{CH,max}} = r_d$ . The rotational factors,  $C_{2,\pm m}^2$ , can be calculated using

$$\langle \cos^2\theta \rangle = \frac{1}{4} \left( 3\cos^2\chi \cos^2\beta + \frac{3}{2} \sin^2\chi \sin^2\beta + \cos^2\beta \right) \quad (37)$$

and

$$\begin{aligned} \langle \cos^4\theta \rangle = & \frac{1}{4} \left( 3\cos^4\chi \cos^4\beta + 9\cos^2\chi \cos^2\beta \sin^2\chi \sin^2\beta \right. \\ & \left. + 3\cos\chi \cos\beta \sin^3\chi \sin^3\beta \right. \\ & \left. + \frac{9}{8} \sin^4\chi \sin^4\beta + \cos^4\beta \right). \end{aligned} \quad (38)$$

The spectral density can be written as

$$J_{\text{m,R,T}}(\omega) = \frac{16\pi n}{15} \int_{r_{\text{CH,min}}}^{r_{\text{CH,max}}} \frac{1}{r_{\text{AX}}^4} \frac{\tau_c/2}{1 + \omega^2 \tau_c^2/4} dr_{\text{AX}}. \quad (39)$$

Finally, Eq. 23 will be used to calculate the relaxation rate. After considering water molecules in different layers to the methyl groups, the total spectral density is the sum of these contributions. When using the average distance between

adjacent water molecules in ice Ih, we found that the relaxation rate due to the second layer is one order of magnitude smaller than that due to the first layer, and the contributions due to the farther layers are insignificant.

## RESULTS AND DISCUSSION

### Experimental $T_1$ values

Each of the CP MAS HPDec  $^{13}\text{C}$  NMR spectra of the four samples, AFP  $i + 4$ , 8 and AFP  $i + 6$ , each frozen in  $\text{H}_2\text{O}$  and  $\text{D}_2\text{O}$ , respectively, only shows a single dominant peak at 16.7 ppm arising from the  $^{13}\text{C}$ -labeled alanine methyl

groups. The intensities of this peak were used to calculate the spin lattice relaxation times. The experimental  $T_1$  values versus the temperatures are given in Fig. 4. These  $T_1$  data are also listed in Table 1, where the subscripts  $\text{H}_2\text{O}$  and  $\text{D}_2\text{O}$  in  $T_{1,\text{H}_2\text{O}}$  and  $T_{1,\text{D}_2\text{O}}$  indicate the corresponding peptides frozen in  $\text{H}_2\text{O}$  and  $\text{D}_2\text{O}$ , respectively. The errors were calculated from fitting the experimental data to the theoretical exponential decay curve shown by Eq. 1. All the relaxation times increased with the increase in temperature, but the extents are larger for the AFP  $i + 4$ , 8 samples. The difference between the  $T_1$  curves for the AFP  $i + 4$ , 8 samples frozen in  $\text{H}_2\text{O}$  and in  $\text{D}_2\text{O}$ , respectively, is clear, but that for the corresponding AFP  $i + 6$  samples is insignificant.

### Methyl group rotation/three-site rotational jump

The dominant mechanisms that govern the Ala methyl  $^{13}\text{C}$  spin lattice relaxation rate for the peptides frozen in  $\text{H}_2\text{O}$  are from the fluctuation of the local dipolar field caused by the

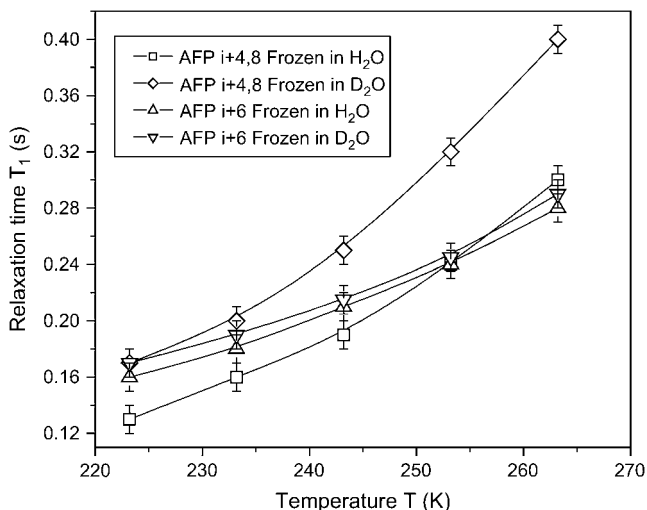


FIGURE 4 Alanine methyl  $^{13}\text{C}$  spin lattice relaxation times versus the temperatures.

methyl group rotation/three-site rotational jump and the reorientations of the proximate water molecules. Thus, the relaxation rate can be written as

$$\frac{1}{T_{1,\text{H}_2\text{O}}} = \frac{1}{T_{1,\text{H}_2\text{O}}^{\text{CH}_3}} + \frac{1}{T_{1,\text{H}_2\text{O}}^{\text{H}_2\text{O}}}, \quad (40)$$

where  $1/T_{1,\text{H}_2\text{O}}^{\text{CH}_3}$  is due to the contribution of the methyl group rotation/three-site rotational jump and  $T_{1,\text{H}_2\text{O}}^{\text{H}_2\text{O}}$  the water molecular reorientation. For the peptides frozen in  $\text{D}_2\text{O}$ , the relaxation rate caused by deuterium is insignificant compared with that by proton. This is because the ratio of the relaxation rates caused by proton and deuterium is estimated to be

$$\frac{1/T_{1,\text{H}_2\text{O}}^{\text{H}_2\text{O}}}{1/T_{1,\text{D}_2\text{O}}^{\text{D}_2\text{O}}} = \frac{\gamma_{\text{H}}^2 I_{\text{H}}(I_{\text{H}} + 1)}{\gamma_{\text{D}}^2 I_{\text{D}}(I_{\text{D}} + 1)} = 15.92, \quad (41)$$

where  $\gamma_{\text{D}}$  and  $\gamma_{\text{H}}$  are the magnetogyric ratios of deuterium (D) and proton (H), respectively, and  $I_{\text{D}}$  and  $I_{\text{H}}$  the corresponding nuclear spin numbers. Therefore, it is estimated that the relaxation rate arose from the methyl group rotation is

$$\frac{1}{T_{1,\text{H}_2\text{O}}^{\text{CH}_3}} \approx \frac{1}{T_{1,\text{D}_2\text{O}}} \quad (42)$$

and the relaxation rate due to  $\text{H}_2\text{O}$ 's reorientation is

$$\frac{1}{T_{1,\text{H}_2\text{O}}^{\text{H}_2\text{O}}} = \frac{1}{T_{1,\text{H}_2\text{O}}} - \frac{1}{T_{1,\text{D}_2\text{O}}}. \quad (43)$$

$T_{1,\text{H}_2\text{O}}^{\text{H}_2\text{O}}$  values at different temperatures for the AFP  $i + 4, 8$  sample are listed in Table 1, and also schematically shown in Fig. 5.  $T_{1,\text{H}_2\text{O}}^{\text{CH}_3}$  values are also given in Fig. 5 for comparison. These data show that methyl group rotation contributes more to the  $^{13}\text{C}$  relaxation rate than the  $\text{H}_2\text{O}$ 's reorientation. Because of the insignificant difference between the relaxation curves for the AFP  $i + 6$  samples frozen in  $\text{H}_2\text{O}$  and  $\text{D}_2\text{O}$ , respectively, the relaxation rate should be primarily determined by the methyl group rotation/three-site rotational jump. These results reveal that the effect on relaxation rates due to water protons to the methyl  $^{13}\text{C}$  nuclei in the 17th and 21st alanine residues is much larger than that to the methyl  $^{13}\text{C}$  nuclei in the 8th, 19th, and 30th alanine residues.

The theoretical  $T_{1,\text{H}_2\text{O}}^{\text{CH}_3}$  curve versus the correlation time  $\tau_c$  for the methyl group rotation/three-site rotational jump is shown in Fig. 6. Eq. 10 was used to calculate the curve, where  $r_{\text{CH}} = 1.07 \text{ \AA}$  was employed (36). The fittings of the experimental  $T_1$  values into the theoretical curve are also given in Fig. 6. The resulting correlation times,  $\tau_{c,\text{CH}_3}$ , are listed in Table 1. The correlation times increased with the decrease in temperature showing the decreased rates of the methyl group rotations at lower temperature. We can also see that the correlation times for the AFP  $i + 4, 8$  sample are longer than those for the AFP  $i + 6$  sample (except the one at  $-50^\circ\text{C}$ ), showing slower methyl group rotations in the AFP  $i + 4, 8$  peptide. Fig. 6 also shows that the spin lattice relaxation times decreased with the increase in their correlation times, indicating that the methyl group rotations/three-site rotational jumps are within in the fast motional limit.

The rotational barrier (activation energy)  $E_a$  for a methyl rotation/three-site rotational jump can be calculated using the Arrhenius equation

$$\log \tau_c = \log \tau_0 + \frac{E_a}{RT}. \quad (44)$$

TABLE 1 Alanine methyl  $^{13}\text{C}$   $T_1$  values (s) and the correlation times (s) of the methyl group rotations/three-site rotational jumps and water molecular reorientation

	$-10^\circ\text{C}$	$-20^\circ\text{C}$	$-30^\circ\text{C}$	$-40^\circ\text{C}$	$-50^\circ\text{C}$
AFP $i + 4, 8$ $T_{1,\text{H}_2\text{O}}$	$0.30 \pm 0.01$	$0.24 \pm 0.01$	$0.19 \pm 0.01$	$0.17 \pm 0.01$	$0.13 \pm 0.01$
AFP $i + 4, 8$ $T_{1,\text{D}_2\text{O}}$	$0.40 \pm 0.02$	$0.32 \pm 0.01$	$0.25 \pm 0.01$	$0.20 \pm 0.01$	$0.17 \pm 0.01$
AFP $i + 4, 8$ $\tau_{c,\text{CH}_3}$	$3.5 \times 10^{-11}$	$4.4 \times 10^{-11}$	$5.6 \times 10^{-11}$	$7.0 \times 10^{-11}$	$8.3 \times 10^{-11}$
AFP $i + 4, 8$ $T_{1,\text{H}_2\text{O}}^{\text{H}_2\text{O}}$	$1.20 \pm 0.02$	$0.96 \pm 0.01$	$0.79 \pm 0.01$	$0.67 \pm 0.01$	$0.55 \pm 0.01$
AFP $i + 4, 8$ $\tau_{c,\text{H}_2\text{O}}$	$1.4 \times 10^{-10}$	$1.8 \times 10^{-10}$	$2.5 \times 10^{-10}$	$3.2 \times 10^{-10}$	$5.2 \times 10^{-10}$
AFP $i + 6$ $T_{1,\text{H}_2\text{O}}$	$0.28 \pm 0.01$	$0.24 \pm 0.01$	$0.21 \pm 0.01$	$0.18 \pm 0.01$	$0.16 \pm 0.01$
AFP $i + 6$ $T_{1,\text{D}_2\text{O}}$	$0.29 \pm 0.01$	$0.25 \pm 0.01$	$0.22 \pm 0.01$	$0.19 \pm 0.01$	$0.18 \pm 0.01$
AFP $i + 6$ $\tau_{c,\text{CH}_3}$	$4.8 \times 10^{-11}$	$5.6 \times 10^{-11}$	$6.5 \times 10^{-11}$	$7.6 \times 10^{-11}$	$8.1 \times 10^{-11}$

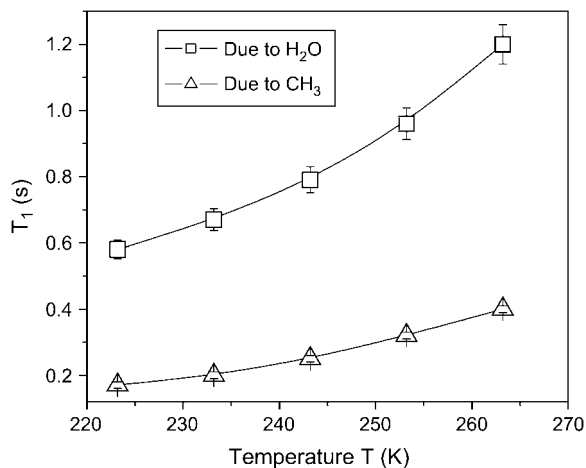


FIGURE 5  $^{13}\text{C}$  relaxation times  $T_{1,\text{H}_2\text{O}}^{\text{CH}_3}$  and  $T_{1,\text{H}_2\text{O}}^{\text{H}_2\text{O}}$  due to the methyl group rotation and the  $\text{H}_2\text{O}$  reorientation, respectively, for the AFP  $i + 4, 8$  sample frozen in  $\text{H}_2\text{O}$  ice.

The  $\log(\tau_c)$  versus  $1/T$  curves are shown in Fig. 7. The corresponding activation energies were found to be  $10.6 \pm 0.6$  kJ/mol for the AFP  $i + 4, 8$  sample, and  $6.7 \pm 0.5$  kJ/mol for the AFP  $i + 6$  sample. The energy barrier for the AFP  $i + 6$  sample is lower than that for the AFP  $i + 4, 8$  sample. This could imply that water molecules interacted with the 17th and 21st alanine methyl groups more closely than water molecules with the 8th, 19th, and 30th alanine methyl groups. A literature value for the torsional barrier of the side-chain methyl group rotation in a crystalline alanine dipeptide is 12.54 kJ/mol (37). The energy barrier for the AFP  $i + 4, 8$  sample is 2 kJ/mol lower than this value. The higher energy barrier indicates a stronger repulsion for the surrounding atoms in the crystal to the methyl hydrogen atoms. In other words, the interaction of the surrounding water molecules with the  $i + 4$  and  $i + 8$  alanine methyl groups for the AFP frozen in ice Ih is weaker than that in a dipeptide crystal.

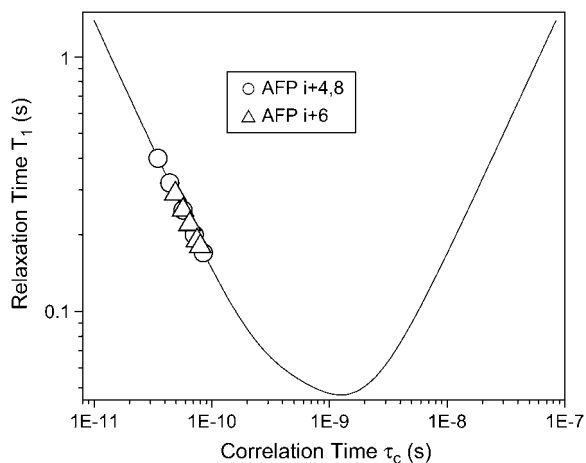


FIGURE 6 Theoretical curve of  $T_{1,\text{H}_2\text{O}}^{\text{CH}_3}$  versus the correlation time  $\tau_c$  and the corresponding experimental  $T_{1,\text{H}_2\text{O}}^{\text{CH}_3}$  values.

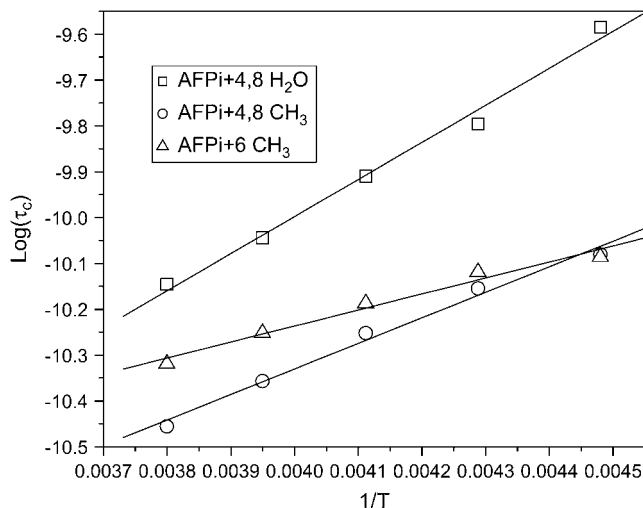


FIGURE 7 Arrhenius plots for the alanine methyl group rotation/three-site rotational jump and the water molecular reorientation for the AFP peptide samples.

### Water surroundings

Equation 39 describes the alanine methyl  $^{13}\text{C}$  spectral density function arising from the reorientation of water molecules in a spherical shell enclosing the methyl group. The shell thickness was taken to be 2.75 Å as the average distance between the adjacent water molecules in ice Ih. As discussed in the theoretical section, we only need to do the calculation up to the second shell. The van der Waals radius of a methyl group is 2.0 Å and that of a hydrogen is 1.2 Å (36). Thus the closest distance for a water proton to approach the carbon nucleus is estimated to be 3.2 Å. Calculation using this distance and the density of ice Ih ( $d_{\text{ice}} = 3.074 \times 10^{28}$  molecules per  $\text{m}^3$ ) results in 13 water molecules in the first shell and 40 water molecules in the second shell. Because a portion of the volume in an ice shell is occupied by the  $\alpha$ -helical peptide, the number of water molecules needs to be reduced. Since the diameter of a standard  $\alpha$ -helix is 5 Å and the average van der Waals radius for carbon, nitrogen, and oxygen atoms is 1.5 Å (36), we choose a cylinder with diameter of 8 Å to exclude the water molecules. We found that 17.78% of the volume is excluded from the first shell and 19.88% from the second shell, which makes the round number for ice molecules to be 10 in the first shell and 33 in the second shell. We define a cube with the edge length to be 0.667 Å to hold a water molecule with the oxygen atom in the center and the two protons in two of the corners to calculate the  $n$  value in Eq. 16. This gives  $n = 6.74943 \times 10^{30}$  protons per  $\text{m}^3$ . To calculate the  $T_1$ - $\tau_c$  curve for the AFP  $i + 4, 8$  sample,  $r_{\text{CH},\text{min}} = r_a$  and  $r_{\text{CH},\text{max}} = r_d$  were used to do the integration of Eq. 39. For comparison, we did three calculations for  $r_{\text{CH},\text{min}} = 3.2$  Å, 3.3 Å, and 3.4 Å. The solid angles taken by the  $\alpha$ -helical AFP have been excluded in the calculation. The resulting theoretical  $T_1$ - $\tau_c$  curves are shown in Fig. 8. The experimental  $T_1$  values are also incorporated

into the corresponding curves. All of the experimental data can fall into the curves for  $r_{\text{CH,min}} = 3.2 \text{ \AA}$  and  $3.3 \text{ \AA}$ , but the lowest  $T_1$  point is off the curve for  $r_{\text{CH,min}} = 3.4 \text{ \AA}$ . More points were found to be off when using longer  $r_{\text{CH,min}}$  values. This indicates that  $r_{\text{CH,min}} = 3.2 \text{ \AA}$ – $3.3 \text{ \AA}$  might be the range of the minimal distance for a water proton in the first shell to the methyl carbon nucleus.  $r_{\text{CH,min}} = 3.2$  corresponds to the van der Waals internuclear distance giving the lowest energy along the axis of the internuclear distance. The corresponding correlation times,  $\tau_{\text{c,H}_2\text{O}}$ , for the water reorientation when using  $r_{\text{CH,min}} = 3.2 \text{ \AA}$  are listed in Table 1. These values increased with the decrease in temperature, showing slower reorientation at lower temperature. Compared with the correlation times of methyl group rotation, these values are much longer. The Arrhenius plot shown in Fig. 7 results in an activation energy of 17.1 kJ/mol. It was found that the energy barrier for water molecular reorientation in ice Ih is 55.8 kJ/mol (35,38,39, and Y. Ba, J. A. Ripmeester, and C. I. Ratcliffe, unpublished), and that in the tetrahydrofuran gas hydrate is 38.8 kJ/mol (Y. Ba, J. A. Ripmeester, and C. I. Ratcliffe, unpublished). Comparison of these data concludes that the mobility of the proximate water molecules to the AFP methyl groups is much higher than those in ice Ih and in tetrahydrofuran gas hydrate, showing that water molecules in the corresponding protein-ice interface were more dynamic than those in the body of ice Ih. The activation energy for water molecular reorientation in the second shell could be higher. However, owing to the much smaller contribution to the total  $T_1$  rate, we ignored the difference in the above calculation.

Because the insignificant difference between the two  $T_1$  curves for the AFP  $i + 6$  samples frozen in  $\text{H}_2\text{O}$  and  $\text{D}_2\text{O}$ , respectively, we were not able to estimate the proximity of water molecules to the methyl carbon atoms. As discussed above, the insignificant difference could be caused by looser water surroundings to the 8th, 19th, and 30th methyl groups, resulting in a lower rotational barrier for the corresponding

methyl group rotations/three-site rotational jumps than that for the 17th and 21st methyl groups. An alternative but less likely interpretation could be that the proximate water molecules are much more dynamic resulting in a much shorter correlation time and a much smaller contribution to the relaxation rate of the 8th, 19th, and 30th methyl group  $^{13}\text{C}$  nuclei. The AFP structure shows that the residues with longer polar and nonpolar side chains, such as Asp, Asn, Leu, and Lys, are toward the  $i + 6$  side in the  $\alpha$ -helical AFP. We think that the pattern of the longer side chains does not fit into the ice lattice well, and could interrupt water molecules to interact with the 8th, 19th, and 30th methyl groups.

## CONCLUSION

It was previously proposed that the ice-binding side of a type I AFP comprises the Thr side chains and the conserved  $i + 4$  and  $i + 8$  Ala residues, where  $i$  indicates the positions of the Thr's commencing the 11 amino acid repeat units. Our  $T_1$  model shows that there could be 10 water molecules closely capping an  $i + 4$  or  $i + 8$  methyl group within the range of van der Waals interaction, whereas the surrounding water molecules to the  $i + 6$  methyl groups could be looser. Thus, the result of the  $^{13}\text{C}$   $T_1$  analysis suggests that the AFP side comprising the  $i + 4$  and  $i + 8$  Ala methyl groups could interact with the ice surface in the ice/water interface. We think that in the ice/water interface, the longer polar side chains are toward the water phase, primarily through hydrogen bonding interaction with water molecules. This could also play a role for the AFP molecules to be driven into the ice/water interface.

This work was supported by National Institutes of Health Minority Biomedical Research Support Program-Score Grant GM08101 and American Chemical Society Petroleum Research Fund No. 39645-GB5M.

## REFERENCES

- DeVries, A. L., and D. E. Wohlschlag. 1969. Freezing resistance in some Antarctic fishes. *Science*. 163:1073–1075.
- Duman, J. G., and A. L. DeVries. 1972. Freezing behavior of aqueous solutions of glycoproteins from the blood of an Antarctic fish. *Cryobiology*. 9:469–472.
- Feeney, R. E., and Y. Yeh. 1978. Antifreeze proteins from fish bloods. *Adv. Protein Chem.* 32:191–282.
- Davies, P. L., and C. L. Hew. 1990. Biochemistry of fish antifreeze proteins. *FASEB J.* 4:2460–2468.
- Evans, R. P., and G. L. Fletcher. 2001. Isolation and characterization of type I antifreeze proteins from Atlantic snailfish (*Liparis atlanticus*) and dusky snailfish (*Liparis gibbus*). *Biochim. Biophys. Acta.* 1547:235–244.
- Duman, J. G. 2001. Antifreeze and ice nucleator proteins in terrestrial arthropods. *Annu. Rev. Physiol.* 63:327–357.
- Worrall, D., L. Elias, D. Ashford, M. Smallwood, C. Sidebottom, P. Lillford, J. Telford, C. Holt, and D. Bowles. 1998. A carrot leucine-rich-repeat protein that inhibits ice recrystallization. *Science*. 282:115–117.
- Sidebottom, C., S. Buckley, P. Pudney, S. Twigg, C. Jarman, C. Holt, J. Telford, A. McArthur, D. Worrall, R. Hubbard, and P. Lillford. 2000. Heat-stable antifreeze protein from grass. *Nature*. 406:256.

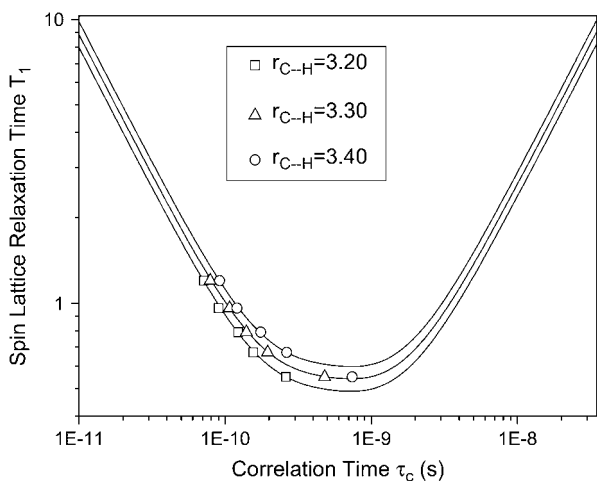


FIGURE 8  $T_{1,\text{H}_2\text{O}}^{\text{H}_2\text{O}}$  theoretical curves versus  $\tau_{\text{c}}$  and the corresponding experimental  $T_{1,\text{H}_2\text{O}}^{\text{H}_2\text{O}}$  values.

9. Harding, M. M., L. G. Ward, and A. D. J. Haymet. 1999. Type I 'antifreeze' proteins. Structure-activity studies and mechanisms of ice growth inhibition. *Eur. J. Biochem.* 264:653–665.
10. Duman, J. G. 1993. Thermal-hysteresis proteins. *Adv. Low Temp Biol.* 2:131–182.
11. Duman, J. G., and A. L. DeVries. 1974. Freezing resistance in winter flounder *Pseudopleuronectes americanus*. *Nature.* 247:237–238.
12. Sicheri, F., and D. S. C. Yang. 1995. Ice-binding structure and mechanism of an antifreeze protein from winter flounder. *Nature.* 375:427–431.
13. Gronwald, W., H. Chao, D. V. Reddy, P. L. Davies, B. D. Sykes, and F. D. Sönnichsen. 1996. NMR characterization of side chain flexibility and backbone structure in the type I antifreeze protein at near freezing temperatures. *Biochemistry.* 35:16698–16704.
14. Sönnichsen, F. D., P. L. Davies, and B. D. Sykes. 1998. NMR structural studies on antifreeze proteins. *Biochem. Cell Biol.* 76:284–293.
15. Raymond, J. A., and A. L. DeVries. 1977. Adsorption inhibition as a mechanism of freezing resistance in polar fishes. *Proc. Natl. Acad. Sci. USA.* 74:2589–2593.
16. Wilson, P. W. 1993. Explanation thermal hysteresis by the Kelvin effect. *Cryo-Letters.* 14:31–36.
17. Knight, C. A., C. C. Cheng, and A. L. DeVries. 1991. Adsorption of alpha-helical antifreeze peptides on specific ice crystal surface planes. *Biophys. J.* 59:409–418.
18. Knight, C. A., and A. L. DeVries. 1994. Effects of a polymeric, nonequilibrium "antifreeze" upon ice growth from water. *J. Cryst. Growth.* 143:301–310.
19. Chao, H., M. E. Houston, Jr., R. S. Hodges, C. M. Kay, B. D. Sykes, M. C. Loewen, P. L. Davies, and F. D. Sönnichsen. 1997. A diminished role for hydrogen bonds in antifreeze protein binding to ice. *J. Biochem. (Tokyo).* 36:14652–14660.
20. Zhang, W., and R. A. Laursen. 1998. Structure-function relationships in a type I antifreeze polypeptide. The role of threonine methyl and hydroxyl groups in antifreeze activity. *J. Biol. Chem.* 273:34806–34812.
21. Haymet, A. D., L. G. Ward, and M. M. Harding. 1999. Winter flounder "antifreeze" proteins: Synthesis and ice growth inhibition of analogues that probe the relative importance of hydrophobic and hydrogen bonding interactions. *J. Am. Chem. Soc.* 121:941–948.
22. Loewen, M. C., H. Chao, M. E. Houston Jr., J. Baardsnes, R. S. Hodges, C. M. Kay, B. D. Sykes, F. D. Sönnichsen, and P. L. Davies. 1999. Alternative roles for putative ice-binding residues in type I antifreeze protein. *Biochemistry.* 38:4743–4749.
23. Baardsnes, J., L. H. Kondejewski, R. S. Hodges, H. Chao, C. Kay, and P. L. Davies. 1999. New ice-binding face for type I antifreeze protein. *FEBS Lett.* 463:87–91.
24. Ba, Y., J. Wongsakhaluang, and J. Li. 2003. Reversible binding of the HPLC6 isoform of Type I antifreeze proteins to ice surfaces and the antifreeze mechanism studied by multiple quantum filtering-spin exchange NMR experiment. *J. Am. Chem. Soc.* 125:330–331.
25. Tulk, C. A., Y. Ba, D. D. Klug, G. McLaurin, and J. A. Ripmeester. 1999. Evidence for phase separation during the crystallization of hyperquenched glassy clathrate hydrate forming solution. *J. Chem. Phys.* 110:6475–6483.
26. Chakrabarty, A., and C. L. Hew. 1991. The effect of enhanced alpha-helicity on the activity of a winter flounder antifreeze polypeptide. *Eur. J. Biochem.* 202:1057–1063.
27. Alamo, R. G., J. A. Blanco, I. Carrilero, and R. Fu. 2002. Measurement of the  $^{13}\text{C}$  spin lattice relaxation time of the non-crystalline regions of semicrystalline polymers by a cp MAS-based method. *Polym.* 43:1857–1865.
28. Torchia, D. A., and A. Szabo. 1982. Spin-lattice relaxation in solid. *J. Magn. Reson.* 49:107–121.
29. Gibby, M. G., A. Pines, and J. S. Waugh. 1972. Anisotropic nuclear spin relaxation of carbon-13 in solid benzene. *Chem. Phys. Lett.* 16: 296–299.
30. Mehring, M., and H. Raber. 1973. Nonexponential spin lattice relaxation and its orientation dependence in a three-spin system. *J. Chem. Phys.* 59:1116–1120.
31. Naito, A., and C. A. McDowell. 1986. Anisotropic behavior of the  $^{13}\text{C}$  nuclear spin dynamics in a single crystal of L-alanine. *J. Chem. Phys.* 84:4181–4185.
32. Bloembergen, N., E. M. Purcell, and R. V. Pound. 1948. Relaxation effects in nuclear magnetic resonance absorption. *Phys. Rev.* 73:679–712.
33. Abragam, A. 1961. *The Principles of Nuclear Magnetism.* The Clarendon Press, Oxford.
34. Harris, R. K. 1985. *Nuclear Magnetic Resonance Spectroscopy,* 1st ed. John Wiley & Sons, New York.
35. Wittebort, R. J., M. G. Usha, D. J. Ruben, D. E. Wemmer, and A. Pine. 1988. Observation of molecular reorientation in ice by proton and deuterium magnetic resonance. *J. Am. Chem. Soc.* 110:5668–5671.
36. Mathews, C. K., and K. E. V. Holde. 1996. *Biochemistry,* 2nd ed. Benjamin Cummings Publishing, Menlo Park, CA.
37. Kneller, G. R., W. Doster, M. Settles, S. Cusack, and J. C. Smith. 1992. Methyl group dynamics in the crystalline alanine dipeptide: A combined computer simulation and inelastic neutron scattering analysis. *J. Chem. Phys.* 97:8864–8879.
38. Auty, R. P., and R. H. Cole. 1952. Dielectric properties of ice and solid  $\text{D}_2\text{O}$ . *J. Chem. Phys.* 20:1309–1314.
39. Granicher, H. 1958. Dielectric relaxation and the electrical conductivity of ice crystals. *Discuss. Faraday Soc.* 23:50–62.